J|A|C|S
ARTICLES
Published on Web 05/04/2004

Projection−Reconstruction Technique for Speeding up Multidimensional NMR Spectroscopy

Ēriks Kupče† and Ray Freeman*,‡

Contribution from the Varian Ltd., 28 Manor Road, Walton-on-Thames, Surrey, KT12 2QF, UK, and Jesus College, Cambridge, CB5 8BL, UK

Received January 31, 2004; E-mail: rf110@hermes.cam.ac.uk

Abstract: The acquisition of multidimensional NMR spectra can be speeded up by a large factor by a projection−reconstruction method related to a technique used in X-ray scanners. The information from a small number of plane projections is used to recreate the full multidimensional spectrum in the familiar format. Projections at any desired angle of incidence are obtained by Fourier transformation of time-domain signals acquired when two or more evolution intervals are incremented simultaneously at different rates. The new technique relies on an established Fourier transform theorem that relates time-domain sections to frequency-domain projections. Recent developments in NMR instrumentation, such as increased resolution and sensitivity, make fast methods for data gathering much more practical for protein and RNA research. Hypercomplex Fourier transformation generates projections in symmetrically related pairs that provide two independent "views" of the spectrum. A new reconstruction algorithm is proposed, based on the inverse Radon transform. Examples are presented of three- and four-dimensional NMR spectra of nuclease A inhibitor reconstructed by this technique with significant savings in measurement time.

Introduction

Multidimensional NMR spectroscopy has proved invaluable for the study of biological molecules, in particular proteins, but is now beginning to reach limits set by the protracted duration of many of these experiments. This is because the traditional methodology involves exploration of all the evolution dimensions independently and with fine digitization. Even when compromises are made with respect to resolution, and when severe restrictions are placed on phase cycling, and even some spectral aliasing is accepted, an expensive NMR spectrometer can be tied up for days at a time by a single investigation. For these reasons several investigators have begun to examine ways to speed up these measurements by more economical schemes for data gathering.[1−20] In many cases the gist of the idea can be traced back to the concept of "accordion spectroscopy"[21] where two evolution parameters were varied simultaneously and in step with one another. Consider a four-dimensional experiment where, in the conventional mode, the evolution dimensions t_1, t_2, and t_3 each require N increments to attain adequate resolution. It can be completed after only N scans by linking t_1, t_2, and t_3 together, a time saving of N^2. If we think of the raw evolution-time data array as a cube, instead of systematically exploring all N^3 data locations, the fast mode simply examines N points lying on the main body diagonal of that cube. This concept has been loosely named "reduced dimensionality".

Naturally there is a price to pay for this speed advantage. First of all, although the sensitivity *per unit time* remains the same, the *overall* sensitivity is reduced in proportion to the square root of the time factor. Fortunately modern high-field spectrometers, particularly those employing a cryogenic receiver coil, often have a high enough intrinsic sensitivity that the final signal-to-noise ratio is still viable. Where sensitivity is marginal, some of the speed advantage must be sacrificed, but the new technique may still be significantly faster than the traditional methodology.

Another feature is the intermodulation that occurs between the different NMR frequencies in the linked evolution dimen-

† Varian Ltd.
‡ Jesus College.

(1) Szyperski, T.; Wider, G.; Bushweller, J. H.; Wüthrich, K. *J. Biomol. NMR* **1993**, *3*, 127−132.
(2) Szyperski, T.; Wider, G.; Bushweller, J. H.; Wüthrich, K. *J. Am. Chem. Soc.* **1993**, *115*, 9307−9308.
(3) Simorre, J.-P.; Brutscher, B.; Caffrey, M.; Marion, D. *J. Biomol. NMR* **1994**, *4*, 325−333.
(4) Brutscher, B.; Simorre, J.-P.; Caffrey, M.; Marion, D. *J. Magn. Reson. B.* **1994**, *105*, 77−82.
(5) Brutscher, B.; Morelle, N.; Cordier, F.; Marion, D. *J. Magn. Reson. B.* **1995**, *109*, 338−242.
(6) Chen, J.; Mandelshtam V. A.; Shaka, A. J. *J. Magn. Reson.* **2000**, *146*, 363−368.
(7) Loening, N. M.; Keeler, J.; Morris, G. A. *J. Magn. Reson.* **2001**, *153*, 103−112.
(8) Szyperski, T.; Yeh, D. C.; Sukumaran, D. K.; Moseley, H. N. B.; Montelione, G. T. *Proc. Natl. Acad. Sci. U.S.A.* **2002**, *99*, 8009−8014.
(9) Ding, K.; Gronenborn, A. *J. Magn. Reson.* **2002**, *156*, 262−268.
(10) Frydman, L.; Scherf, T.; Lupulescu, A. *Proc. Natl. Acad. Sci. U.S.A.* **2002**, *99*, 15859−15862.
(11) Chen, J.; De Angelis, A. A.; Mandelshtam, V. A.; Shaka, A. J. *J. Magn. Reson.* **2003**, *161*, 74−89.
(12) Kim, S.; Szyperski, T. *J. Am. Chem. Soc.* **2003**, *125*, 1385−1393.
(13) Frydman, L.; Lupulescu, A.; Scherf, T. *J. Am. Chem. Soc.* **2003**, *125*, 9204−9217.
(14) Kupče, Ē.; Freeman, R. *J. Magn. Reson.* **2003**, *162*, 300−310.
(15) Kupče, Ē.; Freeman, R. *J. Magn. Reson.* **2003**, *163*, 56−63.
(16) Loening, N. M.; Thrippleton, M. J.; Keeler, J.; Griffin, R. G. *J. Magn. Reson.* **2003**, *164*, 321−328.
(17) Thrippleton, M. J.; Loening, N. M.; Keeler, J. *Magn. Reson. Chem.* **2003**, *41*, 441−447.
(18) Kupče, Ē.; Freeman, R. *J. Biomol. NMR* **2003**, *25*, 349−354.
(19) Kozminski, W.; Zhukov, I. *J. Biomol. NMR* **2003**, *26*, 157−166.
(20) Pelupessy, Ph. *J. Am. Chem. Soc.* **2003**, *125*, 12345−12350.
(21) Bodenhausen, G.; Ernst, R. R. *J. Am. Chem. Soc.* **1982**, *104*, 1304−1309.

sions. Consider a four-dimensional experiment where all three evolution times are varied at the same rate, and where the NMR signal is carried at a frequency Ω_A in the t_1 period, at Ω_B in t_2 and at Ω_C in t_3. At the end of the first evolution interval a signal component $\cos \Omega_A t_1$ is transferred to the second evolution stage t_2. The next transfer is further modulated, involving a component $\cos \Omega_A t_1 \cos \Omega_B t_2$. After the third evolution stage t_3 the signal detected during acquisition is modulated by the terms $\cos \Omega_A t_1 \cos \Omega_B t_2 \cos \Omega_C t_3$. When quadrature detection is employed in all three evolution dimensions, the corresponding sine terms are also detected. Fourier transformation of the appropriate signals generates linear combinations of the individual chemical shifts, as can be appreciated from standard trigonometrical relationships. Signals are modulated at the sum and difference frequencies

$$\Omega_A \pm \Omega_B \pm \Omega_C$$

We shall see below how this intermodulation of chemical shifts affects the results.

Projection−Reconstruction

We describe a method[22−26] for reconstructing the spectra using a processing scheme that is straightforward and transparent. A three-dimensional NMR spectrum is sometimes presented as two stereoscopic views that convey depth perception and give a realistic three-dimensional impression. Evolution by natural selection has determined that two eyes are normally sufficient to take in all the details of a three-dimensional scene; there is no need for systematic scans through all three spatial dimensions. We must moderate this claim when dealing with very crowded NMR spectra where some peaks may be obscured by others in both perspective views, but this problem can be resolved by increasing the number of different projection angles, just as a predatory animal might move laterally to get a better view of its prey. The image of a three-dimensional NMR spectrum is sometimes displayed on a monitor and continuously recomputed so that the entire image appears to rotate about a vertical axis, creating a vivid mental picture of the distribution of absorption peaks in space. These examples suggest that two or more projections of the NMR intensities, taken at different angles of incidence, should provide sufficient information to recreate the entire three-dimensional NMR spectrum. The same principle has been used in X-ray tomography[27] where the problem is considerably more difficult. Because an anatomical specimen is continuous, X-ray tomography requires a large number of projections taken at different angles of incidence, whereas the NMR spectrum is discrete and normally well-resolved, so a much simpler reconstruction procedure is effective. This "PR-NMR" method offers a significant gain in speed by replacing the slow exploration of the evolution dimensions one-by-one by the acquisition of a relatively small number of plane projections. The time saving achieved in a three-dimensional experiment is a function of the number of different projections (P) required for the reconstruction, compared with the much larger number of evolution increments (Q and R) acquired during the two evolution periods in the conventional mode. Time constraints oblige the operator to keep Q and R as small as possible, consistent with resolution requirements; they would typically be 64 and 128 in a 900 MHz spectrometer. Suppose that a three-dimensional projection−reconstruction experiment varies t_1 and t_2 simultaneously in Q steps and acquires P different projections. The speed advantage would be R/P, which could easily be an order of magnitude, reducing a day-long experiment to about an hour. The improvement in measurement time is correspondingly higher for four-dimensional spectra. This allows spectra to be recorded for unstable biomolecules or permits the exploration of time-dependent phenomena such as relaxation or slow chemical exchange. Alternatively, it can significantly improve the relatively poor resolution imposed on conventional multidimensional spectroscopy by measurement time constraints.

A connection with GFT-NMR[12] emerges when we consider how the tilted projections are derived. There is a Fourier transform theorem[28,29] which states that a section through a two-dimensional time-domain signal $S(t_1,t_2)$ running through the origin and subtending an angle, α with respect to the t_1 axis transforms as the projection of the two-dimensional frequency-domain signal $S(F_1,F_2)$ onto a line through the origin subtending the same angle α with respect to the F_1 axis. The important concept is readily extended to a three-dimensional spectrum where projection onto a tilted *plane* is achieved by Fourier transformation of a signal recorded while t_1 and t_2 are varied simultaneously at rates defined by

$$t_1 = t \cos \alpha \quad (1)$$

$$t_2 = t \sin \alpha \quad (2)$$

(During the third time interval t_3, the NMR signal is acquired in real time in the normal manner.) The tilted projection plane is rotated through an angle α with respect to the F_1F_3 plane. (F_3 is the direct detection axis and remains invariant in these experiments.) The key to the PR-NMR method is this ability to select any desired orientation for the projection plane by varying the evolution times at different rates.

Consider first the special case $t_2 = 0$ ($\alpha = 0°$) where Fourier transformation of the signal $S(t_1)$ generates a projection onto the F_1F_3 plane (Figure 1a). Similarly transformation of $S(t_2)$ for the special case $t_1 = 0$ ($\alpha = 90°$) generates a projection onto the orthogonal F_2F_3 plane (Figure 1b). These are commonly known as the "first planes" and are often used during the experimental setting-up procedure. One might speculate whether these two orthogonal projections alone would suffice to reconstruct the three-dimensional spectrum. Unfortunately, except in very simple cases, some ambiguities remain because the number of independent measurements of projected intensity is less than the total number of potential cross-peaks. Further tilted projections are required to augment the intensity information and eliminate ambiguity. Indeed, for very complex spectra more than one choice of tilt angle may be required. Hence the importance of incrementing the evolution parameters t_1 and t_2 at *different* rates.

(22) Freeman, R.; Kupče, Ē. *J. Biomol. NMR* **2003**, *27*, 101−113.
(23) Kupče, Ē.; Freeman, R. *J. Biomol. NMR* **2003**, *27*, 383−387.
(24) Kupče, Ē.; Nishida, T.; Freeman, R. *Prog. Nucl. Magn. Reson. Spectrosc.* **2003**, *42*, 95−122.
(25) Kupče, Ē.; Freeman, R. *J. Am. Chem. Soc.* **2003**, *125*, 13958−13959.
(26) Kupče, Ē.; Freeman, R. *J. Biomol. NMR* **2004**, *28*, 391−395.
(27) Hounsfield, G. N. *Br. J. Radiol.* **1973**, *46*, 1016.
(28) Bracewell, R. N. *Aust. J. Phys.* **1956**, *9*, 198.
(29) Nagayama, K.; Bachmann, P.; Wüthrich, K.; Ernst, R. R. *J. Magn. Reson.* **1978**, *31*, 133.

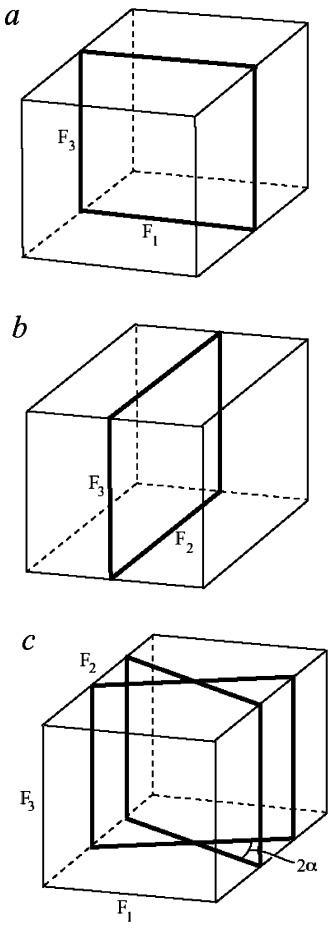

Figure 1. Various possible projection planes (bold lines) of a three-dimensional spectrum. (a) If $t_2 = 0$ ($\alpha = 0°$) the projection plane is F_1F_3. (b) If $t_1 = 0$ ($\alpha = 90°$) the projection plane is F_2F_3. (c) If t_1 and t_2 are varied simultaneously at different rates, hypercomplex Fourier transformation generates two projections, tilted through angles $\pm\alpha$ about the F_3 (direct detection) axis.

Projection-reconstruction takes care of the chemical shift intermodulation effect in a straightforward manner. Consider a three-dimensional PR-NMR experiment where the real and imaginary signal components are excited in both evolution dimensions[21] giving four modulation terms:

$$S_1 = \cos(\Omega_A t \cos\alpha)\cos(\Omega_B t \sin\alpha) \quad (3)$$

$$S_2 = \cos(\Omega_A t \cos\alpha)\sin(\Omega_B t \sin\alpha) \quad (4)$$

$$S_3 = \sin(\Omega_A t \cos\alpha)\cos(\Omega_B t \sin\alpha) \quad (5)$$

$$S_4 = \sin(\Omega_A t \cos\alpha)\sin(\Omega_B t \sin\alpha) \quad (6)$$

Standard trigonometric transformations give the quadrature components:

$$S_1 - S_4 = \cos(\Omega_A t \cos\alpha + \Omega_B t \sin\alpha) \quad (7)$$

$$S_2 + S_3 = \sin(\Omega_A t \cos\alpha + \Omega_B t \sin\alpha) \quad (8)$$

$$S_1 + S_4 = \cos(\Omega_A t \cos\alpha - \Omega_B t \sin\alpha) \quad (9)$$

$$S_2 - S_3 = \sin(\Omega_A t \cos\alpha - \Omega_B t \sin\alpha) \quad (10)$$

Consequently the standard hypercomplex Fourier transformation (see the Supporting Information) of these combinations generates the sum and difference frequencies:

$$(\Omega_A \cos\alpha + \Omega_B \sin\alpha) \text{ and } (\Omega_A \cos\alpha - \Omega_B \sin\alpha)$$

These involve *differential scaling* of the chemical shifts, reflecting the extent to which the projection plane is tilted through the arbitrary angle α. Note that the existence of sum and difference frequencies simply means that there are *two* tilted projections, making angles $\pm\alpha$ with respect to the F_1F_3 plane (Figure 1c). These provide two independent views of the three-dimensional spectrum, and both contribute to solving the reconstruction problem.

Overlap, which can cause ambiguities in the NMR spectroscopy of large bio-molecules, can be avoided by the appropriate choice of tilt angle. This can be appreciated in a three-dimensional HNCO experiment on isotopically labeled ubiquitin, where the tilt angle is varied systematically in 10° steps (Figure 2). Each of the four absorption peaks follows a separate trajectory, tracing out a smooth sinusoidal path. It is clear that any exact frequency degeneracies are few and far between and can be readily avoided by the choice of tilt angle. In fact this is the only significant intervention required of the operator, and it can be automated if necessary (see below).

Line Widths. In large biological molecules, the instrumental line width due to field inhomogeneity can often be neglected in comparison with the broader natural line widths. The various nuclear species involved in a three-dimensional experiment may well have significantly different rates of spin−spin relaxation and consequently different natural line widths. Let the relaxation time be T_2^A in the t_1 evolution dimension and T_2^B in the t_2 dimension. In an experiment where t_1 and t_2 are varied simultaneously, the transverse relaxation is given by

$$M(t) = M_0 \exp(-t_1/T_2^A)\exp(-t_2/T_2^B) \quad (11)$$

For a tilted projection where $t_1 = t\cos\alpha$ and $t_2 = t\sin\alpha$, this expression becomes

$$M(t) = M_0 \exp[-t(\cos\alpha/T_2^A + \sin\alpha/T_2^B)] \quad (12)$$

and an effective spin−spin relaxation time can be defined as

$$T_2^{\text{eff}} = T_2^A T_2^B/(T_2^B \cos\alpha + T_2^A \sin\alpha) \quad (13)$$

corresponding to an effective full Lorentzian line width at half-height

$$\Delta\nu = 1/(\pi T_2^{\text{eff}}) = \cos\alpha/(\pi T_2^A) + \sin\alpha/(\pi T_2^B) \quad (14)$$

Thus, in tilted projections the lines are always broader than those in at least one of the orthogonal projections. In cases where T_2^A is longer than T_2^B, it is an advantage to select a small tilt angle since this favors the more slowly relaxing *A* spins. However in practice there are more important factors governing the choice of tilt angle, notably the desire to avoid overlap of peaks in a given projection direction. These results presuppose conventional incrementation of the evolution in both t_1 and t_2. In a "constant-time" experiment, the corresponding relaxation term disappears and the line width is determined by an artificial broadening function and the results of linear prediction.

Reconstruction of the Spectrum

Multidimensional spectra are characterized by a set of "cross-peak" resonances correlating the NMR responses of the various

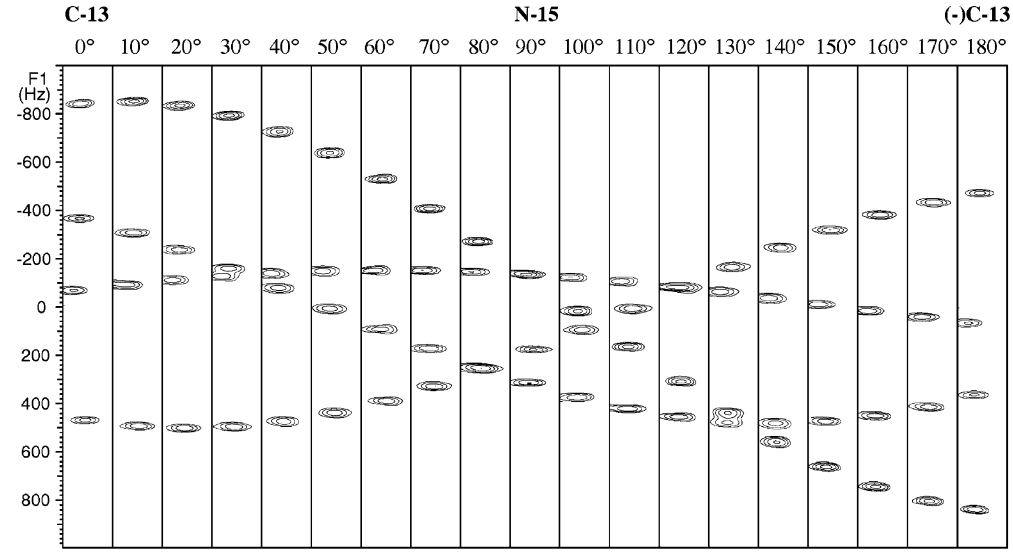

Figure 2. Projections of a selected section of the three-dimensional HNCO spectrum of ubiquitin onto planes that are progressively tilted in 10° increments starting from the carbon-proton plane, running through the nitrogen-proton plane (center) and back to the carbon-proton plane. Each of the four cross-peaks follows a sinusoidal trajectory with relatively few exact frequency degeneracies with other cross-peaks, suggesting that the selection of the tilt angle is not particularly critical.

chemical sites. They are generated by coherence or magnetization transfer during a sequence of consecutive evolution periods. The observed resonance frequencies are represented as coordinates in multidimensional space. Viewed as an "image" to be reconstructed, the NMR spectrum is made up of discrete features that are well resolved and have well-characterized shapes. In this respect, it is less challenging than a physiological sample studied by X-ray tomography, where the density function is a continuum. The reconstruction treatment reduces to finding the unique multidimensional array of NMR peaks compatible with all the measured plane projections.

Reconstruction methods are used in electron microscopy, geophysical exploration, ultrasonics, X-ray tomography, and magnetic resonance imaging. Often the inverse Radon transform[30,31] is involved. Projections involve the integration of the absorbed intensity along a series of parallel beams through the sample, and the Radon transform calculates these line integrals. Usually the angle of incidence of the beams is varied in uniform steps around a circle, and the corresponding projections are acquired.

$$R(p, \phi) = \int\int f(x, y)\, \delta(x \cos \phi + y \sin \phi - p)\, \mathrm{d}x\, \mathrm{d}y \quad (15)$$

where p is the perpendicular distance of the beam from the origin and ϕ is the angle of incidence of the beams. In practice it is the inverse Radon transform that is of interest for reconstructing NMR spectra.

$$f(x, y) = \int p(x \cos \phi + y \sin \phi, \phi)\, \mathrm{d}\phi \quad (16)$$

It uses the information in the projections to reconstruct the image $f(x, y)$.

There are several possible approaches to the challenging task of finding a two- or three-dimensional density function compatible with all the measured projections. Some invoke an iterative fitting procedure, and others are best described as "back projection". Two alternative approaches are described here; the choice depends on the intrinsic sensitivity of the sample to be investigated.

Spectra with Good Sensitivity. Spectra with good inherent sensitivity favor a processing scheme based on only few projections. The starting point is the pair of orthogonal projections on the F_1F_3 and F_2F_3 planes. A three-dimensional array $S(F_1, F_2, F_3)$ is reconstructed by processing one F_1F_2 plane at a time. In a typical F_1F_2 plane, the raw experimental data for $\alpha = 0°$ and $\alpha = 90°$ are one-dimensional absorption spectra, representing the projections of NMR intensity onto the F_1 and F_2 axes (Figure 3a). As mentioned above, ambiguity arises because the information in the two orthogonal projections is not normally sufficient to determine all the cross-peak intensities. For example, M projected peaks along the F_1 axis and N projected peaks along the F_2 axis contain insufficient information to determine the intensities at MN intersections, unless M and N are very small numbers.

However it is a simple matter to derive a *provisional* map that defines all the *possible* cross-peak coordinates. Some of these locations correspond to actual peaks, and others will later turn out to be unoccupied. This provisional map is obtained by a two-dimensional convolution of the one-dimensional F_1 and F_2 traces. However, since both projections are delta functions in one of the two dimensions, this reduces to a simple scaling of the intensities in one trace according to the corresponding ordinate in the orthogonal trace. The result is a spectrum of cross-peaks in the F_1F_2 plane in which every peak in the F_1 projection appears to be correlated with every peak in the F_2 projection. In Figure 3a, there are three peaks in each projection, giving rise to nine *potential* cross-peaks.

To resolve the ambiguities, complementary information is taken from additional projections tilted at $\pm\alpha$, intersecting at a skew angle (Figure 1c). This imposes new intensity constraints and identifies the genuine cross-peaks. For simplicity, consider the effect of one such tilted projection made up of just two responses. This trace is back-projected, creating a two-dimensional "mask" consisting of two parallel ridges running across the F_1F_2

(30) Deans, S. R. *The Radon Transform and Some of its Applications*, 1983, Wiley: New York.
(31) Kupče, E.; Freeman, R. *Concepts Magn. Reson.* **2004**, in press

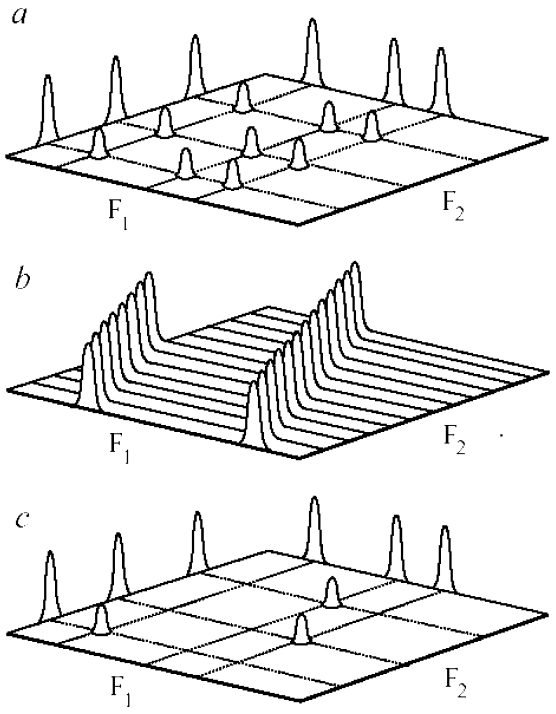

Figure 3. (a) A provisional (F_1F_2) spectrum is created by convolution of the projections on the F_1 and F_2 axes. Not all of these nine locations represent genuine cross-peaks. The "false" correlations are eliminated by introducing information from a tilted projection. (b) A "mask" is created by back-projection of the tilted projection, generating parallel ridges, in this case two in number. This mask is superimposed on spectrum a and intensities at corresponding locations compared; retaining the lower intensity at each point. (c) This eliminates peaks not overlapped by the ridges, leaving only three genuine correlation peaks.

plane at a skew angle (Figure 3b). This mask is superimposed on the provisional spectrum of cross-peaks (Figure 3a) and the intensities at each location are compared and replaced by the lower value.[32,33] In this manner, unless the ridges intersect one of the provisional cross-peaks, the latter is eliminated (Figure 3c). In this example only three of the nine potential cross-peaks turn out to be genuine. The corresponding projection at $-\alpha$ introduces a further constraint that serves to resolve any remaining ambiguities. In most practical situations, a single iteration suffices to identify all the true correlations, but for very complex spectra, any remaining ambiguity can be resolved by recording a second pair of projections at a different tilt angle.

The lower-value algorithm is a nonlinear processing operation but the practical drawbacks are normally quite mild - - a possible slight loss in peak intensities and a tendency to reduce the baseplane noise level in regions not covered by the ridges. More serious consequences are anticipated for spectra with a poor signal-to-noise ratio, but this operational mode, like most fast multidimensional experiments, is predicated on good intrinsic sensitivity. Note that the accumulation of more projections does not increase the signal intensity in this mode. A trivial artifact of the lower-value algorithm is the imposition of some polygonal character on the intensity contours, the number of edges being twice the number of tilted projections employed. Once all such F_1F_2 planes have been processed, the three-dimensional spectrum is complete and can be displayed in any of the usual formats.

Spectra with Poor Sensitivity. In this situation it is an advantage to record a rather larger number of different projections. A related problem is faced by a sculptor setting out to create an "image" in the form of a three-dimensional solid. Rodin, for example, always worked with a live model, and he would arrange for the model to be backlit in order to observe a silhouette. The model posed on a turntable that could be rotated in small angular increments, to generate a number of silhouettes from slightly different perspectives. In this manner Rodin obtained enough spatial information to be able to sculpt a true likeness.

The PR-NMR technique differs only in that the projections represent variable absorption intensities, whereas the sculptor's silhouettes were made up of rectangular functions, either zero or unit intensity. A relatively large number of different NMR projections are recorded, usually spaced uniformly around a circle as in the Radon transform methodology. Instead of the lower-value algorithm, reconstruction is achieved by *adding* the contributions from the many different back-projections. There is strong reinforcement of intensity at positions of genuine NMR peaks, enhancing the sensitivity in proportion to the number of different projections. This is an advantage as long as the number of projections remains smaller than the number of evolution increments in the conventional mode. All reduced dimensionality methods lose their advantages in the sensitivity-limited regime.

This additive scheme creates some residual artifacts, low intensity ridges and weak "ghost" peaks where these ridges intersect, features that are compatible with some, but not all, of the projections. Fortunately genuine cross-peaks are readily identified because they fall at locations where all the ridges intersect, whereas artifacts always involve fewer intersections. The larger the number of independent projections, the weaker these artifacts become in relation to the cross-peaks. The effect of increasing the number of projections is illustrated in spectra shown in the Supporting Information. Note that this method of reconstruction may slightly modify the line shape.

This additive approach is preferred over the lower-value method in situations where the intrinsic signal-to-noise ratio is poor because each new projection enhances the final signal intensities, and the weak artifacts tend to sink below the general noise level. Under these conditions it is better to enhance the signal-to-noise ratio by sampling the time-domain signals at more closely spaced angles of incidence (where each measurement is independent of the others) than to employ multiscan averaging (where the same signals are sampled over and over again).

An illustrative example is shown in Figure 4, taken from the 500 MHz three-dimensional HN(CA)CO spectrum of ubiquitin, which has characteristically poor sensitivity. The time-domain signals in the evolution dimensions were recorded for 64 increments and extended by linear prediction to 128 complex points and then zero-filled to 512 complex points. The F_1F_3 plane (Figure 4a) has poor sensitivity, and a transverse section at a proton frequency of 8.3 ppm was deliberately chosen as an illustration (the noisy trace shown along the top margin). The corresponding F_1F_2 plane (Figure 4b) was then remeasured from

(32) Baumann, R.; Wider, G.; Ernst, R. R.; Wüthrich, K. *J. Magn. Reson*. **1981**, *44*, 402.
(33) McIntyre, L.; Wu, X.-L.; Freeman, R. *J. Magn. Reson*. **1990**, *87*, 194−201.

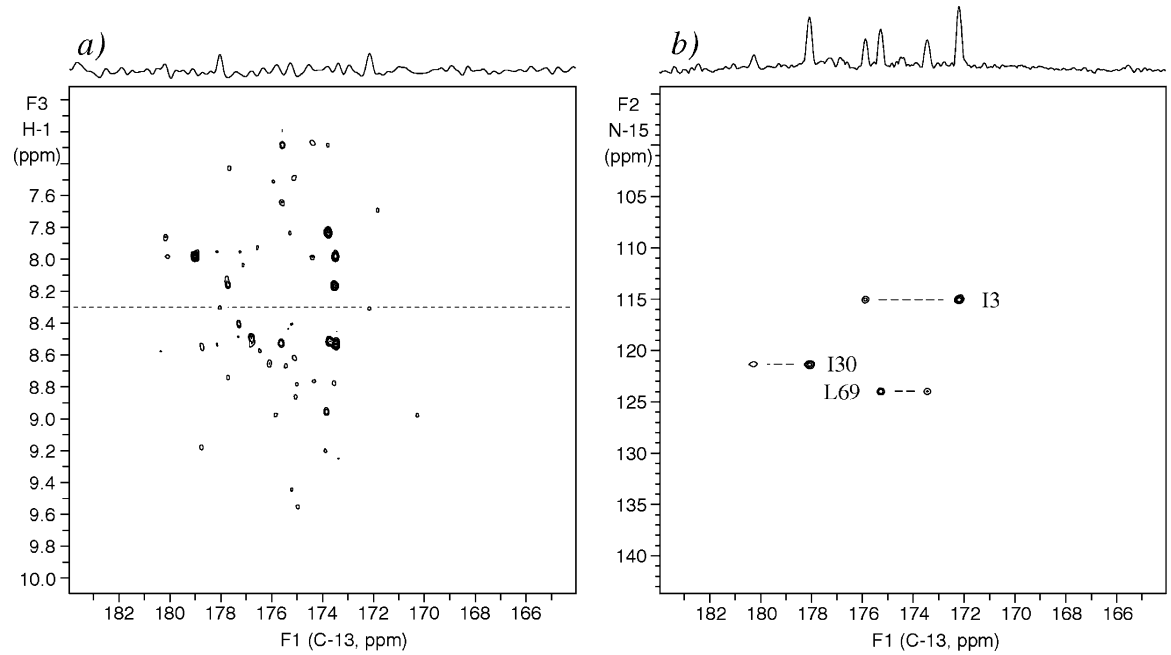

Figure 4. Improvement in sensitivity achieved by adding back-projections. (a) A selected F_1F_3 plane from the three-dimensional HN(CA)CO spectrum of ubiquitin uniformly labeled with carbon-13 and nitrogen-15. A trace at $F_3 = 8.3$ ppm (top margin) was selected on the grounds of low signal-to-noise ratio. (b) The corresponding F_1F_2 plane obtained from a reconstructed three-dimensional spectrum that recorded 18 planes inclined at regular intervals from −80° to +90°. The projected trace (top margin) illustrates the sensitivity enhancement, allowing three correlations to be detected.

a spectrum reconstructed from a set of projections taken at 18 different angles of incidence (0°, ±10°, ±20°, ±30°, ±40°, ±50°, ±60°, ±70°, ±80°, 90°). The back-projections were added together to enhance the signal-to-noise ratio, and because of the large number of projections, the artifacts mostly disappeared into the general baseplane noise. This sensitivity improvement (of the order of $\sqrt{18}$) allowed the three correlations shown in Figure 4b to be clearly revealed. Similar principles apply to the inverse Radon transform applied to four-dimensional spectra.

Selection of a Suitable Tilt Angle. The information contained in the orthogonal F_1F_3 and F_2F_3 planes of a three-dimensional spectrum is limited, in the sense that it generates only a *provisional* lattice of cross-peaks, some of which are actual and some false. It can nevertheless be used to predict a suitable tilt angle for the next stage of the reconstruction, without having to record any further experimental data. As described above, F_1F_2 planes are processed one at a time by convoluting the projections on the F_1 and F_2 axes. This provisional two-dimensional array is then projected onto a line tilted at an angle α. Along each individual projection beam the highest intensity is retained (rather than the more usual integral) so that if two or more peaks are eclipsed, the projected intensity corresponds to only a *single* peak. A count (P) is then made of all the projected peaks for this tilt angle. If overlap occurs along any of the beams, this reduces the count P. The calculation of P is repeated for a series of values of α between ±90°, generating a graph of P versus α that has dips whenever α corresponds to eclipsed cross-peaks (actual or false). The corresponding graphs of P against α for all the other F_1F_2 planes are then summed together (ΣP). A suitable setting for the tilt angle α is any point on this graph of ΣP that avoids these dips in intensity. Once an appropriate tilt angle has been chosen and a tilted projection obtained, the next stage of the reconstruction eliminates the majority of "false" correlations, and a new graph of ΣP against tilt angle maps mainly cases of *actual* overlap. Then a new and more reliable assessment of a suitable tilt angle can be made for the next stage of the reconstruction. The method works best for spectra that are not too complex.

Line Shapes. Consider the two orthogonal projections where $\alpha = 0°$ and 90°. Convolution of these two traces generates the correct two-dimensional line shape in the frequency domain (provided that the resonances are resolved). In large biochemical molecules, these will be determined by the natural (rather than instrumental) line widths. Figure 5b is an illustration of spectral line shapes obtained by two-dimensional convolution, compared with the rectangular contours imposed by application of the lower-value algorithm (Figure 5a). Another example (a three-dimensional HNCA spectrum) is shown in the Supporting Information. Good line shapes are important for measurements of spin−spin coupling constants from partially resolved splittings, in this case carbon−carbon doublets. Consequently all the important features of the NMR spectrum, intensities, frequency coordinates, line width, and line shape, are available in a reconstructed spectrum.

Accuracy of Chemical Shift Determination. Procedures for sequential assignment of protein spectra rely on reasonably accurate values for the chemical shifts. In PR-NMR, chemical shifts can be measured by least-squares fitting of the resonance lines recorded on the orthogonal projections, just as in a conventional experiment. As for all such measurements, the accuracy is dependent on line width, fineness of digitization, and signal-to-noise ratio. There is no reason to think that the PR-NMR method displaces these resonance frequencies or distorts the symmetry of the line shape. Consequently, if reasonable precautions are taken to ensure adequate digitization, the accuracy is predicted to be equivalent to that of the conventional mode at the same sensitivity level. If necessary, resolution can be increased by extending the evolution periods, at the expense of some sacrifice in the speed factor.

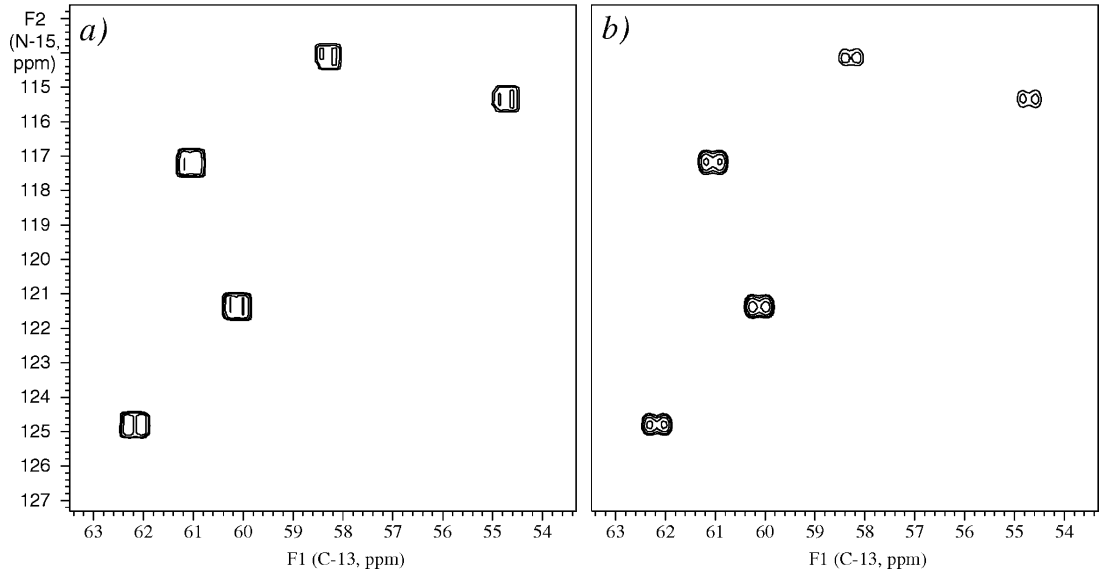

Figure 5. Line shapes in reconstructed three-dimensional HN(CO)CA spectra of isotopically labeled ubiquitin, showing C−C doublets. (a) When the lower-value algorithm is used, the intensity contours are approximately rectangular. (b) When the convolution method is employed, the contours reflect the line shapes recorded in the orthogonal dimensions. Faithful reproduction of the line shape can be important for the accurate determination of spin−spin splittings.

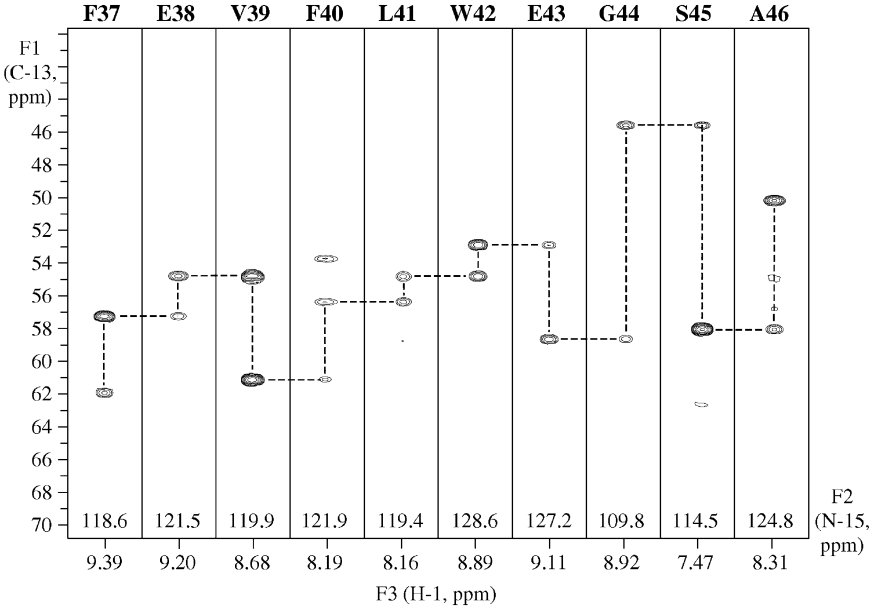

Figure 6. Strip plots from the 800 MHz three-dimensional HNCA spectrum of nuclease A inhibitor (a 3 mM aqueous solution, 10% D_2O at 25 °C) reconstructed from projections recorded at ±30° and ±60°. The duration of the signal in the evolution period was doubled by linear prediction and extended by another factor of 4 by zero-filling. The correlations between nitrogen-15 and carbon-13 sites define a chain running from residue 37 to residue 46, terminated by proline residues, with a missing response from residue 47.

Applications to Three-Dimensional Spectra. Initial feasibility tests[23−25] have already confirmed the applicability of projection−reconstruction for three-dimensional NMR spectra of protein samples. As a practical illustration we chose the important HNCA experiment, widely used to provide sequential connectivities in proteins by correlating the amide proton and nitrogen-15 chemical shifts with the intraresidue Cα shift via the N−C direct coupling, and with the Cα shift of the preceding residue via the two-bond N−C coupling. Typically these connectivities are demonstrated in terms of a "walkthrough" of the residues in the form of a strip plot (Figure 6). The PR-NMR method has the distinct advantage that it displays the result in the conventional form. High-field studies are particularly beneficial for PR-NMR, and for this reason, the three-dimensional HNCA spectrum was examined in an 800 MHz spectrometer. The sample was the carbon-13- and nitrogen-15-labeled nuclease A inhibitor,[37] consisting of 143 residues. The nitrogen-proton projection was "borrowed" from the corresponding N-15 HSQC experiment. The three-dimensional spectrum was reconstructed from two orthogonal projections,

(34) Kay, L. E.; Ikura, M.; Tschudin, R.; Bax, A. *J. Magn. Reson.* **1990**, *89*, 496−514.
(35) Kay, L. E.; Xu, G. Y.; Yamazaki, T. J. *J. Magn. Reson. A* **1994**, *109*, 129−133.
(36) Ottiger, M.; Delaglio, F.; Bax, A. *J. Magn. Reson.* **1998**, *131*, 373−378.
(37) Kirby, T. W.; DeRose, E. F.; Mueller, G. A.; Meiss, G.; Pingoud, A.; London, R. E. *J. Mol. Biol.* **2002**, *320*, 771−782.

and four tilted projections were recorded at ±30° and ±60° corresponding to evolution times in the ratios of 0.577 and 1.732, respectively. All projections were derived from 64 time-domain increments, extended to 128 points by linear prediction, and zero-filled to 512 complex points, with four scans per increment. The strip plot of Figure 6 maps the nine N−Cα correlations along a chain terminated by the proline residues P-36 and P-48. The response from residue 47 is missing.[37] The measurement time was 10 min per projection, giving a total experimental duration of 1 h. It is estimated that the corresponding duration of a conventional three-dimensional measurement (with 64 and 32 time-domain increments) would be 11 h.

Four-Dimensional Spectroscopy. Four-dimensional experiments are often employed when there is ambiguity in the corresponding three-dimensional spectra. They can be speeded up by an appreciably larger factor by projection−reconstruction. A third evolution period (t_3) is introduced, the real and imaginary components are excited in all three evolution dimensions, and then the NMR response is acquired during the direct detection stage (t_4). It is still possible to visualize the problem pictorially by concentrating on the three evolution dimensions F_1, F_2, and F_3, the "evolution subspace" (Figure 7). The direct-detection dimension F_4 is not shown.

There are now three evolution times that may be incremented independently, or simultaneously in pairs, or all together. A new tilt angle β is introduced in a more general formulation that reduces to the earlier one if $\beta = 0°$.

$$t_1 = t \cos \alpha \cos \beta \tag{17}$$

$$t_2 = t \sin \alpha \cos \beta \tag{18}$$

$$t_3 = t \sin \beta \tag{19}$$

The angle α defines a rotation about the F_3 axis (Figure 7a), while β represents rotation about a general axis in the F_1F_2 plane (Figure 7c). The direct projection planes are defined by the F_4 axis and one of these vectors in evolution subspace. There are now three categories of projection to be considered, orthogonal, tilted, and doubly tilted.

Orthogonal Projections. Consider, first of all, the projections onto the three "first planes" F_1F_4, F_2F_4, and F_3F_4. The positions of peaks in one such plane are not affected by the peak positions in the other (orthogonal) planes. Note that in this *four-dimensional* problem, these projection planes cannot be illustrated in the diagram (Figure 7) but must be imagined. By setting $t_2 = t_3 = 0$ ($\alpha = 0°$, $\beta = 0°$) and incrementing t_1, the projection onto the F_1F_4 plane is obtained. Setting $t_1 = t_3 = 0$ ($\alpha = 90°$, $\beta = 0°$) and incrementing t_2 gives the F_2F_4 projection. Setting $t_1 = t_2 = 0$ ($\alpha = 0°$, $\beta = 90°$) and incrementing t_3 gives the F_3F_4 projection. These might, for example, represent H(N)CO(CA), H(NCO)CA, and HN(COCA) spectra, respectively.

In the general case, these three orthogonal projections do not provide enough information to solve the entire problem because of accidental overlap of cross-peaks along the projection directions, as discussed above for three-dimensional spectra. However these orthogonal planes do offer certain advantages. They can be recorded independently and, in suitable cases, can be "borrowed" from a related experiment. The chemical shifts are recorded rather more accurately than those derived from tilted projections where the observed frequencies are scaled down by the cosine or sine factors.

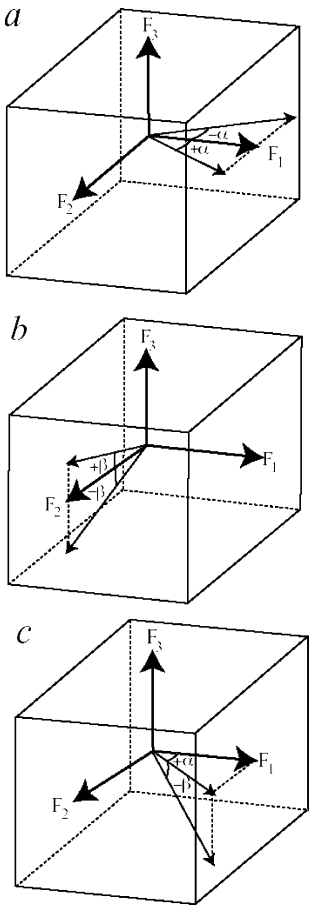

Figure 7. "Evolution subspace" of a four-dimensional NMR experiment; the direct detection dimension (F_4) has to be imagined. (a) If the timing parameters t_1 and t_2 are incremented together at different rates while $t_3 = 0$, the spectrum is projected onto two tilted planes defined by ±α and the F_4 axis. (b) If t_2 and t_3 are incremented together while $t_1 = 0$, the projection planes are defined by ±β and the F_4 axix. (c) If t_1, t_2, and t_3 are incremented simultaneously, there are two pairs of doubly-tilted projection planes defined by ±α and ±β and the F_4 axis. For reasons of clarity, only the axis defined by +α and −β is shown here.

Tilted Projections. The next category of projection measurement allows two of the three evolution parameters to vary in step while the third is held at zero. There are three kinds of tilted projection. If t_1 and t_2 are incremented simultaneously with $t_3 = 0$, this corresponds to an arbitrary tilt angle α in the F_1F_2 plane with $\beta = 0°$. It represents a pair of symmetrically related projection planes defined by ±α and the F_4 axis (Figure 7a). If t_1 and t_3 are varied jointly, while $t_2 = 0$, the corresponding projection planes are tilted through angles ±β in the F_1F_3 plane with $\alpha = 0°$. If t_2 and t_3 are linked together while $t_1 = 0$, the resulting projection planes are tilted through angles ±β in the F_2F_3 plane with $\alpha = 90°$ (Figure 7b).

Doubly Tilted Projections. Finally there are the "doubly tilted" projections recorded when all three evolution parameters t_1, t_2, and t_3 are varied simultaneously. Both α and β are now involved (Figure 7c). Eight different responses are recorded, switching between radio frequency phase 0° and 90° in each of the three evolution dimensions. There are now eight terms modulating the signal detected during t_4.

Phase	Modulating Signal	
0° 0° 0°	$S_1 = \cos(\Omega_A t \cos\alpha \cos\beta)$ $\cos(\Omega_B t \sin a \cos\beta) \cos(\Omega_C t \sin\beta)$	(20)
0° 0° 90°	$S_2 = \cos(\Omega_A t \cos\alpha \cos\beta)$ $\cos(\Omega_B t \sin a \cos\beta) \sin(\Omega_C t \sin\beta)$	(21)
0° 90° 0°	$S_3 = \cos(\Omega_A t \cos\alpha \cos\beta)$ $\sin(\Omega_B t \sin a \cos\beta) \cos(\Omega_C t \sin\beta)$	(22)
0° 90° 90°	$S_4 = \cos(\Omega_A t \cos\alpha \cos\beta)$ $\sin(\Omega_B t \sin a \cos\beta) \sin(\Omega_C t \sin\beta)$	(23)
90° 0° 0°	$S_5 = \sin(\Omega_A t \cos\alpha \cos\beta)$ $\cos(\Omega_B t \sin a \cos\beta) \cos(\Omega_C t \sin\beta)$	(24)
90° 0° 90°	$S_6 = \sin(\Omega_A t \cos\alpha \cos\beta)$ $\cos(\Omega_B t \sin a \cos\beta) \sin(\Omega_C t \sin\beta)$	(25)
90° 90° 0°	$S_7 = \sin(\Omega_A t \cos\alpha \cos\beta)$ $\sin(\Omega_B t \sin a \cos\beta) \cos(\Omega_C t \sin\beta)$	(26)
90° 90° 90°	$S_8 = \sin(\Omega_A t \cos\alpha \cos\beta)$ $\sin(\Omega_B t \sin a \cos\beta) \sin(\Omega_C t \sin\beta)$	(27)

Hypercomplex Fourier transformation (see Supporting Information) of the appropriate combinations generates doubly tilted projection planes defined by the F_4 axis and the directions $[+\alpha, +\alpha]$, $[+\alpha, -\beta]$, $[-\alpha, +\beta]$, and $[-\alpha, -\beta]$, providing four independent views of the four-dimensional NMR spectrum. For example, standard trigonometry shows that the combination $S_1 - S_4 - S_6 - S_7$ corresponds to a modulation term:

$$\cos(\Omega_A t \cos\alpha \cos\beta + \Omega_B t \sin\alpha \cos\beta + \Omega_C t \sin\beta)$$

and the combination $S_2 + S_3 + S_5 - S_8$ gives the corresponding quadrature component:

$$\sin(\Omega_A t \cos\alpha \cos\beta + \Omega_B t \sin\alpha \cos\beta + \Omega_C t \sin\beta)$$

Fourier transformation with respect to t gives the sum of the projected chemical shifts:

$$(\Omega_A \cos\alpha \cos\beta + \Omega_B \sin\alpha \cos\beta + \Omega_C \sin\beta)$$

This corresponds to the projection of the four-dimensional spectrum onto a plane defined by $[+\alpha, +\beta]$ and the F_4 axis. Analogous manipulations yield the terms:

$$(\Omega_A \cos\alpha \cos\beta - \Omega_B \sin\alpha \cos\beta + \Omega_C \sin\beta)$$

$$(\Omega_A \cos\alpha \cos\beta + \Omega_B \sin\alpha \cos\beta - \Omega_C \sin\beta)$$

$$(\Omega_A \cos\alpha \cos\beta - \Omega_B \sin\alpha \cos\beta - \Omega_C \sin\beta)$$

Intermodulation of the chemical shift frequencies has generated four projection planes, symmetrically related in two pairs, just as the three-dimensional case gave two projection planes tilted at $\pm\alpha$. The scaling simply reflects the orientation of these doubly tilted planes; during processing they are rotated back to the appropriate orthogonal plane so that the superposition algorithm can be reapplied and the true cross-peaks identified.

The GFT-NMR technique[12] also involves three separate categories of signals recorded by linking the evolution dimensions of a four-dimensional experiment, but the subsequent data treatment is quite distinct, being purely algebraic. In the usual practice, the three rates of incrementation are kept equal so there is no differential scaling of chemical shifts. The raw experimental signals are processed in the time domain by a G-matrix transform which is a general extension of the sum and difference rule used for processing three-dimensional spectra. Subsequent Fourier transformation gives linear combinations of chemical shifts as shown above, from which the "pure" chemical shifts are extracted by a peak-picking routine and a least-squares fitting procedure. The G-matrix transform in the time domain (followed by Fourier transformation) is now seen to be equivalent to the standard hypercomplex Fourier transformation of the appropriate combinations of quadrature signals used in PR-NMR.

This highlights the importance of incrementing the evolution times at different rates, thereby defining tilt angles $\pm\alpha$ and $\pm\beta$ that can cover all possible projection directions. The selection of a suitable tilt angle is not critical. There is no reason to think that $\alpha = 45°$ is the best choice, but it is preferable to avoid angles too close to 0° or 90° because these projections are too similar to the orthogonal ones.

The PR-NMR results are presented as sections through the four-dimensional spectrum in the familiar format. Standard radio frequency pulse sequences are used, with no significant changes except the linking of the evolution times together and possibly modification of the first few data points in the evolution dimensions to take account of the slightly shorter dwell times in the PR-NMR mode. These sequences are available from several pulse program libraries, such as the Varian BioPack, and because of their complexity, most NMR spectroscopists simply take them on trust. PR-NMR is therefore directly applicable to an entire range of familiar multidimensional experiments. The only innovation is in the data processing.

Experimental Procedure

The task is to establish the most efficient experimental procedure and optimum dimensionality for such correlation experiments, bearing in mind the possibility of degeneracies in chemical shifts. The first point to note is that some correlations are obtained *directly*, that is to say they involve the direct-detection dimension, while others are inferred *indirectly*. For example, in a four-dimensional PR-NMR experiment, the direct projection planes are F_1F_4, F_2F_4, and F_3F_4. By contrast, the three planes F_1F_2, F_2F_3, and F_1F_3 in the evolution subspace correspond to indirect correlations. This distinction may be represented schematically as a tetrahedron showing the direct correlations as solid lines and the indirect ones as dotted lines (Figure 8b).

The most exciting application of multidimensional NMR spectroscopy is the study of protein structure, often using samples uniformly labeled in carbon-13 and nitrogen-15, with one of many standard pulse sequences.[34−39] Normally the heteronuclear carbon-13 and nitrogen-15 spins are excited only indirectly, while the detected response is that of the proton, usually in an NH group. In many cases there is no simple way to obtain a direct correlation between the two heteronuclear species, for example, carbon-13 and nitrogen-15, or between Cα and C═O.

(38) Yamazaki, T.; Lee, W.; Arrowsmith, C. H.; Muhandiram, D. R.; Kay, L. E. *J. Am. Chem. Soc.* **1994**, *116*, 11655−11666.
(39) Yang, D.; Kay, L. *J. Am. Chem. Soc.* **1999**, *121*, 2571−2575.

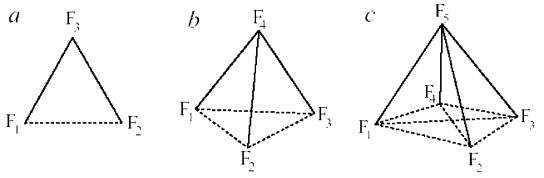

Figure 8. Schematic representation of multidimensional spectroscopy (a) in three dimensions, (b) in four dimensions, and (c) in five dimensions. Correlations are divided into direct (solid lines) and indirect (dashed) lines. This representation makes it possible to predict the minimum number of experiments required to derive all the correlation information, even in cases of ambiguity. For example, comparison of parts a and c demonstrates that a five-dimensional problem can be solved by six separate three-dimensional measurements.

Furthermore these different categories of experiment are usually treated independently, although it has been shown[23] that economies of measurement time can be achieved by "borrowing" an orthogonal projection from one experiment (HNCO) to use in a second type of experiment (HN(CO)CA). This strategy is demonstrated below for a four-dimensional spectrum.

Consider a typical four-dimensional PR-NMR experiment. Suppose there are two degenerate chemical shifts in the F_4 dimension, so that there are two projection peaks along each of the F_1, F_2, and F_3 axes of the evolution subspace. This ambiguity predicts eight *possible* locations for the cross-peaks. Subsequent projection onto two pairs of doubly tilted planes provides sufficient new information to identify the two genuine cross-peaks. This raises the important general question of the minimum number of projections required to solve the reconstruction problem for multidimensional spectra and the related matter of the most efficient procedure to achieve this goal. In general, overlap can occur in any dimension, so projections onto all six orthogonal planes (F_1F_2, F_2F_3, F_1F_3, F_1F_4, F_2F_4, and F_3F_4) must be recorded to be certain that all possible ambiguities are resolved.

The schematic representations of Figure 8 give important clues about the best procedure. They predict, for example, that all the information contained in a conventional four-dimensional experiment could be obtained from a set of three conventional three-dimensional experiments involving the dimensions $F_1F_2F_4$, $F_2F_3F_4$, and $F_1F_3F_4$.

The PR-NMR treatment of a four-dimensional problem might reconstruct each of the three-dimensional spectra from one direct orthogonal projection, for example, onto the F_1F_4 plane, and three pairs of tilted projections. Alternatively the same result can be achieved more efficiently by exploiting the set of four doubly tilted projection planes, which provide all the required indirect connectivity information, $F_1 \rightarrow F_2$, $F_1 \rightarrow F_3$, and $F_2 \rightarrow F_3$. This choice is predicated on the assumption that the experimental duration is the critical parameter.

Applications to Four-Dimensional Spectroscopy. The projection−reconstruction technique is demonstrated for a four-dimensional HNCOCA experiment performed on isotopically labelled nuclease A inhibitor, a 143-residue protein, investigated on a Varian 600 MHz spectrometer equipped with a cryogenic receiver coil. The first step is to record a three-dimensional HNCO experiment. Figure 9a shows one F_1F_2 plane (carbon−nitrogen correlations) at a fixed proton frequency of 8.55 ppm. This contains seven cross-peaks, and the task is to assign them by means of four-dimensional PR-NMR measurements.

The next step is to record the three orthogonal "first planes" F_1F_4, F_2F_4, and F_3F_4 of the four-dimensional HNCOCA experiment. Instead of recording the usual F_3F_4 and F_1F_4 projections, the equivalent information was "borrowed" from a two-dimensional nitrogen-15 HSQC experiment (which enjoys a roughly 4-fold advantage in sensitivity) and from the three-dimensional HNCO experiment (with a roughly 2-fold gain in sensitivity). Most protein investigations would involve these preliminary experiments in any case. The F_2F_4 first plane was recorded in the normal fashion by incrementing t_2, keeping t_1 and t_3 held at zero. With time averaging of just two transients, each of these experiments required 5 min of data gathering. All the remaining information was obtained by recording four doubly tilted projections where t_1, t_2, and t_3 were incremented simultaneously, with $\alpha = \pm 45°$ and $\beta = \pm 45°$. This required another 20 min of data gathering, giving a total of 35 min for the entire measurement. It is estimated that a full conventional four-dimensional experiment would have required about 4 days of data accumulation.

Figure 9b assigns the seven responses of Figure 9a according to their Cα frequencies which are spread out in the F_2 dimension. The six different F_1F_3 planes are overlaid, with the correlations identified by color-coding. The two blue peaks fall in the same Cα plane and cannot be distinguished from this information. Figure 9c spreads out the seven responses in six different F_2F_3 planes according to their CO frequencies, with the two magenta peaks falling in the same plane. Figure 9d spreads the same seven responses into six different F_1F_2 planes according to their nitrogen-15 frequencies, identified by color-coding, with Leu-133 and Thr-138 (orange) falling in the same plane. These results demonstrate that the four-dimensional information can be obtained by projection−reconstruction methods with a roughly 160-fold speed advantage over the traditional HNCOCA methodology.

Five-Dimensional Spectra. Large proteins usually relax too fast to permit realistic five-dimensional experiments, but five-dimensional spectroscopy of smaller molecules is still feasible. It requires an extension of the analysis to take account of four consecutive evolution intervals, t_1, t_2, t_3, and t_4, while the fifth dimension t_5 corresponds to direct detection in real time. The correlations can be divided into direct and indirect as illustrated by the solid and dotted lines of a tetragonal pyramid (Figure 8c). When there is ambiguity, all six dotted correlations are required. This way of formulating the problem is important because it predicts alternative pathways to the final result. It shows, for example, that all the information in a five-dimensional spectrum can be extracted from a set of six separate three-dimensional measurements involving the "triangular" correlations:

$$F_1 \rightarrow F_2 \rightarrow F_5$$
$$F_2 \rightarrow F_3 \rightarrow F_5$$
$$F_3 \rightarrow F_4 \rightarrow F_5$$
$$F_1 \rightarrow F_3 \rightarrow F_5$$
$$F_1 \rightarrow F_4 \rightarrow F_5$$
$$F_2 \rightarrow F_4 \rightarrow F_5$$

Alternatively a set of four separate four-dimensional experiments would provide all 10 required correlations or two four-dimensional experiments and one three-dimensional measurement.

In the five-dimensional case, a new rotation angle γ is introduced and the expressions for the tilt angles α and β are reformulated (although the new equations reduce to the earlier ones when $\gamma = 0°$). The four evolution times are varied at rates given by

$$t_1 = t \cos\alpha \cos\beta \cos\gamma \quad (28)$$
$$t_2 = t \sin\alpha \cos\beta \cos\gamma \quad (29)$$
$$t_3 = t \sin\beta \cos\gamma \quad (30)$$
$$t_4 = t \sin\gamma \quad (31)$$

Consider the case where all four evolution times are incremented simultaneously. This involves permutation of the radio frequency phase (0° or 90°) in all four evolution dimensions. Hypercomplex Fourier transformation of the appropriate combinations of signals generates eight

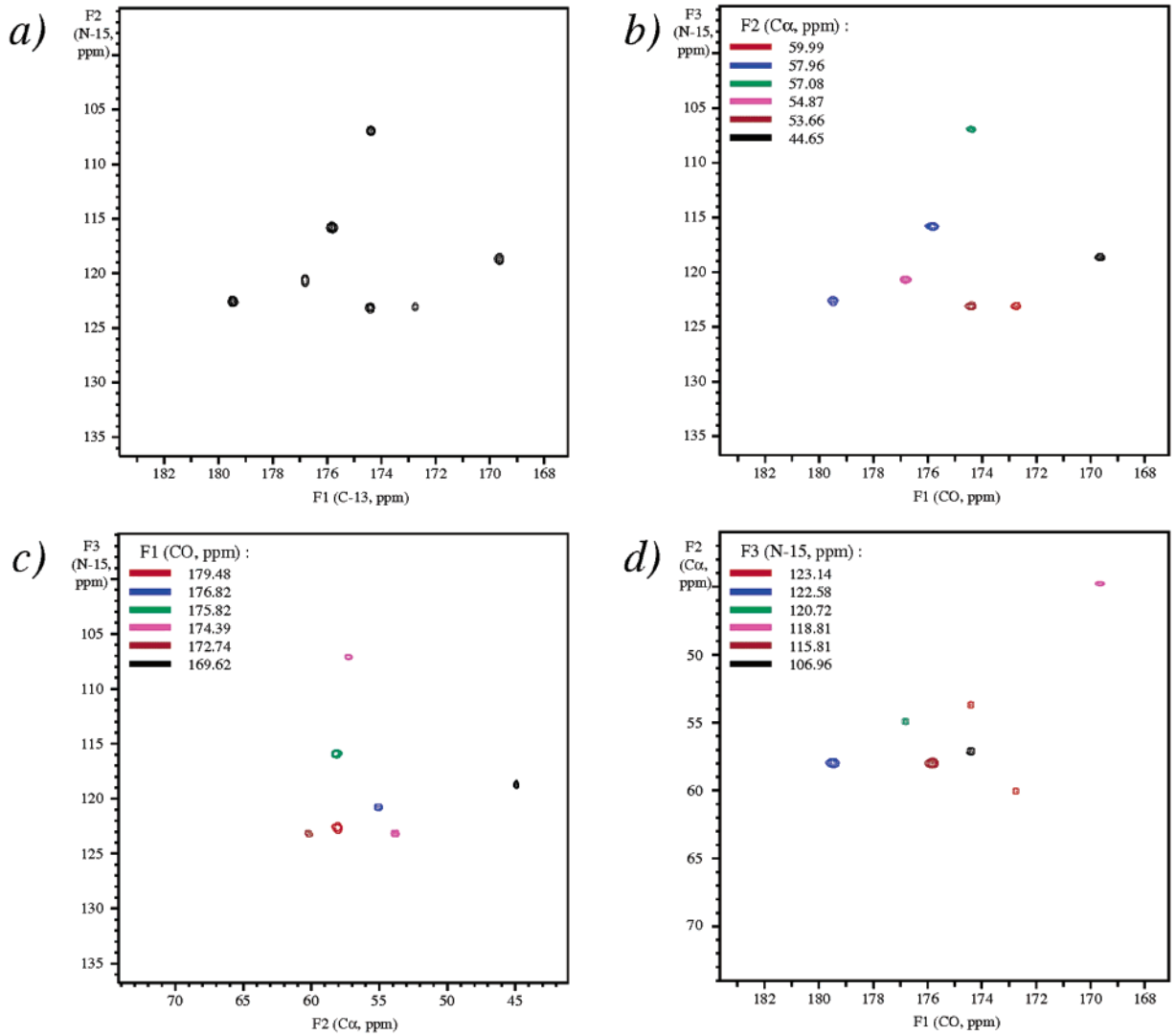

Figure 9. Projection−reconstruction of a 600 MHz four-dimensional HNCOCA spectrum of 3 mM nuclease A inhibitor on the basis of three orthogonal projections F_1F_4, F_2F_4, and F_3F_4 and four doubly tilted projections defined by $\alpha = \pm 45°$ and $\beta = \pm 45°$ and the F_4 axis. (a) A preliminary three-dimensional HNCO experiment, showing seven carbon−nitrogen correlations in an F_1F_2 plane at a fixed proton frequency of 8.55 ppm. (b) The four-dimensional experiment where these peaks are spread into six different F_1F_3 planes according to the Cα frequencies; the two blue peaks fall in the same plane. (c) Spreading into six different F_2F_3 planes according to the CO frequencies; the two magenta peaks fall in the same plane. (d) Spreading into six different F_1F_2 planes according to the nitrogen-15 frequencies; the two orange peaks fall in the same plane. In this plane, the peaks can be assigned as Leu-133 and Thr-138 (orange), Leu-20 (blue), Glu-86 (green), Gly-126 (magenta), Gln-62 (brown), and His-60 (black).

triply tilted projection planes defined by the F_5 axis and the eight directions $[\pm\alpha, \pm\beta, \pm\gamma]$. These projections involve sums and differences of four (projected) chemical shift terms:

$$\Omega_A \cos\alpha \cos\beta \cos\gamma \pm \Omega_B \sin\alpha \cos\beta \cos\gamma \pm \Omega_C \sin\beta \cos\gamma \pm \Omega_D \sin\gamma$$

There are four categories of doubly tilted projections. For example, if t_4 is held at zero ($\gamma = 0°$) while t_1, t_2, and t_3 are varied simultaneously, there are planes defined by the F_5 axis and the directions $[\pm\alpha, \pm\beta]$. In all there are 16 different doubly tilted projection planes. There are six categories of singly tilted projections; for example, if t_3 and t_4 are zero ($\beta = \gamma = 0°$) while t_1 and t_2 are incremented in concert, the projection planes are defined by the F_5 axis and the directions $[\pm\alpha]$. This gives 12 possible projection planes. The mode with the shortest duration would be to measure the eight triply tilted complex planes. A practical demonstration of five-dimensional PR-NMR has just appeared.[40] Extension to even higher dimensions is perfectly feasible but of little practical importance at the present time.

Discussion

Provided that sensitivity is not a limiting factor, it is clear that multidimensional NMR spectroscopy can be speeded up by linking the evolution periods together, rather than by varying them independently. We propose that the clearest way to interpret such results is as a set of tilted projections of the spectrum in the frequency domain, relying on a well-established Fourier transform theorem. This allows the full spectrum to be reconstructed by finding the only multidimensional array of absorption peaks that is compatible with the measured projections. The analogy with stereoscopic vision makes it clear how the method works in practice and emphasizes the importance of choosing a good "point of view" set by the relative rates of incrementation of the evolution parameters. Intermodulation of chemical shift frequencies, originally thought to be an undesir-

(40) Coggins, B. E.; Venters, R. A.; Zhou, P. *J. Am. Chem. Soc.* **2004**, *126*, 1000−1001.

able complication in the data processing, simply means that the projections are acquired in symmetrically related pairs at positive and negative tilt angles. The PR-NMR method promises to extend the scope of protein studies and to open the door to the investigation of time-dependent phenomena such as relaxation[41] or slow chemical exchange.

Acknowledgment. Spectra were recorded by remote operation on Varian 600 and 800 MHz spectrometers in Palo Alto, California; the authors are indebted to George Gray, Mark Van Criekinge, Carl Carter, and Knut Mehr for practical help in setting up these experiments. The authors thank Thomas W. Kirby, Eugene F. DeRose, Geoffrey A. Mueller, Gregor Meiss, Alfred Pingoud, and Robert E. London for the sample of nuclease A inhibitor.[37]

Supporting Information Available: (I) Line shape in reconstructed three-dimensional HNCA spectrum of ubiquitin. (II) Base-plane artifacts in reconstructed three-dimensional HN(CA)-CO spectrum shown in Figure 4b. (III) Hypercomplex Fourier transformation of the tilted planes in projection reconstruction NMR. This material is available free of charge via the Internet at http://pubs.acs.org.

JA049432Q

(41) Kay, L. Private communication.